Photonic band-gap engineering in UV fiber gratings by the arc discharge technique

Andrea Cusano[1*], Agostino Iadicicco[2], Domenico Paladino[1], Stefania Campopiano[2], and Antonello Cutolo[1]

[1]Optoelectronic Division-Engineering Department, University of Sannio, Corso Garibaldi 107, 82100 Benevento, Italy
[2] Department for Technologies, University of Naples Parthenope, Centro Direzionale Napoli, Isola C4, 80143 Napoli, Italy
**Corresponding author: a.cusano@unisannio.it*

Abstract: Localized heat treatments combined with local non-adiabatic tapering is proposed as suitable tool for the engineering of photonic band-gaps in UV-written fiber Bragg gratings (FBGs). In particular, here, we propose the use of the electric arc discharge to achieve localized defects along the FBG structure, however differently from previously reported works, we demonstrate how this post processing tool properly modified can be exploited to achieve the full control of the spectral characteristics of the final device. Also, we show how the suitable choice of the grating features and the correct selection of the defect geometry can be efficiently used to achieve interesting features for both communication and sensing applications.

OCIS codes: (050.2770) Gratings; (060.2340) Fiber optics components; (230.3990) Microstructure devices; (350.2660) Fusion.

References and links

1. J. D. Joannopoulos, R. D. Meade, and J. N. Winn, *Photonic Crystals. Molding the Flow of Light*, (Princeton University Press, Princeton, NJ, 1995).
2. S. Fan, P. R. Villeneuve, J. D. Joannopoulos, H. A. Haus, "Channel drop filters in photonic crystals," Opt. Express **3**, 4-11 (1998).
3. I. Del Villar, I. R. Matías, F. J. Arregui, R. O. Claus, "Fiber-optic nanorefractometer based on one-dimensional photonic-bandgap structures with two defects," IEEE Trans. Nanotechnol. **3**, 293-299 (2004).
4. T. Asano, M. Mochizuki, S. Noda, M. Okano, M. Imada, "A channel drop filter using a single defect in a 2-D photonic crystal slab-defect engineering with respect to polarization mode and ratio of emissions from upper and lower sides," J. Lightwave Technol. **21**, 1370-1376 (2003).
5. L. Wei, J. W. Y. Lit, "Phase-shifted Bragg grating filters with symmetrical structures," J. Lightwave Technol. **15**, 1405-1410 (1997).
6. F. Bakhti, P. Sansonetti, "Design and realization of multiple quarter-wave phase-shifts UV-written bandpass filters in optical fibers," J. Lightwave Technol. **15**, 1433-1437 (1997).
7. R. Kashyap, P. F. McKee, D. Armes, "UV written reflection grating structures in photosensitive optical fibers using phase-shifted phase-masks," Electron. Lett. **30**, 1977–1979 (1994).
8. Y. Sheng, J. E. Rothenberg, H. Li, Y. Wang, J. Zweiback, "Split of phase shifts in a phase mask for fiber Bragg gratings," IEEE Photon. Technol. Lett. **16**, 1316-1318 (2004).
9. J. Canning, M. G. Sceats, "π-phase-shifted periodic distributed structures in optical fibers by UV post-processing," Electron. Lett. **30**, 1344-1345 (1994).
10. M. Janos, J. Canning, "Permanent and transient resonances thermally induced in optical fibre Bragg gratings," Electron. Lett. **31**, 1007-1009 (1995).
11. D. Uttamchandani, A. Othonos, "Phase shifted Bragg gratings formed in optical fibres by post-fabrication thermal processing," Opt. Commun. **127**, 200-204 (1996).
12. A. Iadicicco, A. Cusano, S. Campopiano, A. Cutolo, M. Giordano, "Microstructured fiber Bragg gratings: analysis and fabrication," Electron. Lett. **41**, 466-468 (2005).
13. A. Iadicicco, S. Campopiano, A. Cutolo, M. Giordano, A. Cusano, "Refractive index sensor based on microstructured fiber Bragg grating," IEEE Photon. Technol. Lett. **17**, 1250-1252 (2005).
14. A. Cusano, A. Iadicicco, D. Paladino, S. Campopiano, A. Cutolo, M. Giordano, "Micro-structured fiber Bragg gratings. Part I: Spectral characteristics," Opt. Fiber Technol. **13**, 281-290 (2007).

#97128 - $15.00 USD Received 5 Jun 2008; revised 30 Jul 2008; accepted 30 Jul 2008; published 15 Sep 2008

15. A. Cusano, A. Iadicicco, D. Paladino, S. Campopiano, A. Cutolo, M. Giordano, "Micro-structured fiber Bragg gratings. Part II: Towards advanced photonic devices," Opt. Fiber Technol. **13**, 291-301 (2007).
16. M. Pisco, A. Iadicicco, S. Campopiano, A. Cutolo, A. Cusano, "Micro-structured chirped fiber Bragg gratings: towards new spatial encoded fiber optic sensors," Proc. SPIE **6619**, 66192T (2007).
17. A. Iadicicco, S. Campopiano, D. Paladino, A. Cutolo, A. Cusano, "Micro-structured fiber Bragg gratings: optimization of the fabrication process," Opt. Express **15**, 15011-15021 (2007).
18. D. Paladino, A. Iadicicco, S. Campopiano, A. Cutolo, A. Cusano, "Nonlithographic fabrication of microstructured fiber Bragg grating evanescent wave sensors," Proc. SPIE **7003**, 70031Z (2008).

1. Introduction

The novel and unique way to control many features of the electromagnetic radiation by opportune photonic band-gap (PBG) structures have inspired a lot of interest and many research efforts have been devoted to their possible applications [1]. These artificial structures are characterized by one, two or three-dimensional (1D, 2D or 3D) periodic arrangements of dielectric material that have a band-gap that forbids propagation of a certain frequency range of light. This property enables one to control light with amazing facility and produce novel appealing effects for optical communications [2] and sensing applications [3]. In the last years, the inclusion of one or more defects in a PBG structure has been widely investigated because of the spectral properties it presents. Defects break the structure symmetry and may give rise to a defect state or allowed frequency within the PBG region [4].

Among the large variety of PBG structures, great attention has been focused in the last decades on Fiber Bragg Gratings (FBGs) which can be considered 1D PBGs realised within optical fibers by UV writing. However, to meet the increasing demand in high performance photonic devices, great efforts have been devoted to develop simple methods to tailor the spectral features of these devices by the inclusion of defects breaking the grating periodicity. For instance, FBGs with single or multiple phase shifts at various precise locations along the grating have been proposed for creating narrow spectral resonances for both filtering and laser applications [5-6].

These structures can be produced at the fabrication stage by using specially designed phase masks incorporating the required phase shifts with restrictions on the magnitude, position, and number [6-8]. However, the cost of this procedure, the dependence on the operating wavelength and the need of a large variety of phase masks to produce structures with different and optimised spectral properties for specific applications are the major limitations of this approach.

To overcome this problem, many researchers focused their attention on the development of post processing techniques able to induce distributed phase shifts along the grating structure enabling the tailoring of the band-gap features.

On this line of arguments, Canning et al. demonstrated the fabrication of a π-phase-shifted grating by local UV post-exposure, however also in this case the post processing technique requires the use of complex equipment and expensive tools [9]. Some years later, photonic band-gap engineering of fiber gratings was demonstrated by post-fabrication thermal treatments using localised heating [10-11]. The erasure of a short region of the grating creates in fact a distributed phase shift or equivalently a Fabry-Perot like structure whereas the lateral gratings act as wavelength selective reflectors separated by a delay segment corresponding to the erased region [11]. However in both single- and two-defect configurations, only weak defect states were achieved due to the unbalance of the lateral mirrors due to unwanted errors in the phase shift position, limiting the effective potentiality of the post processing approach to achieve a full tailoring of the spectral characteristics of the final device.

Recently the authors presented a novel FBG configuration involving micro-structured fiber Bragg gratings (MSFBGs) and employing localized defects along the grating region realized by post processing local structuration of the host fiber [12-13]. The perturbation consists in the stripping of the cladding layer in a well defined region along the grating structure. The perturbation acts as a distributed phase shift with the consequent formation of a defect state inside the stop-band spectrum similarly to the effect observed in phase shift gratings (PSGs) [14]. Differently from previous configurations, MSFBGs exhibit a spectral

#97128 - $15.00 USD Received 5 Jun 2008; revised 30 Jul 2008; accepted 30 Jul 2008; published 15 Sep 2008

response dependent on the surrounding refractive index (SRI), able to tune the defect state within the grating stop-band and enabling the possibility to realize new and attractive passive and active photonics devices [14-16]. Also convenient post processing methodologies involving lithographic and not-lithographic procedures have been demonstrated [17-18]. However the extreme flexibility of this structure related to SRI-based tuning mechanism has the main drawback in the significant weakening of the final structure due to the deep thinning of the host fiber.

In light of this limitation, here we focus the attention on the thermal post processing treatment realised by the arc discharge technique to improve the capability of performing photonic band-gap engineering in fiber grating devices written by UV exposure.

In particular, here, we propose the use of the electric arc discharge (EAD) to achieve localized defects along the FBG structure similarly to Ref. [11], however differently from Ref. [11], we demonstrate how this post processing tool properly modified can be exploited to achieve the full control of the spectral characteristics of the final device. Also, we show how the suitable choice of the grating features and the correct selection of the defect geometry can be efficiently used to achieve interesting features for both communication and sensing applications.

2. Methodology

The aim of this work is the proper use of the EAD technique as post processing tool to obtain a complete control of the photonic band-gap modifications in fiber grating devices realized by UV exposure. With reference to the structure in Fig. 1(a), the spectral position of the defect state inside the original grating band-gap (see Fig. 1(b)) depends on the distributed phase shift induced by the erased region which, in turn, depends on the cavity length (L_C) and the effective refractive index (n_C) of the fundamental mode.

According to PSGs theory, a central defect state versus the grating stop-band is possible if the induced phase shift is π+/-2k π, where k is an integer. Moreover, the depth of the defect state only depends on the balance between the cavity mirrors corresponding to the lateral and unperturbed grating regions [14].

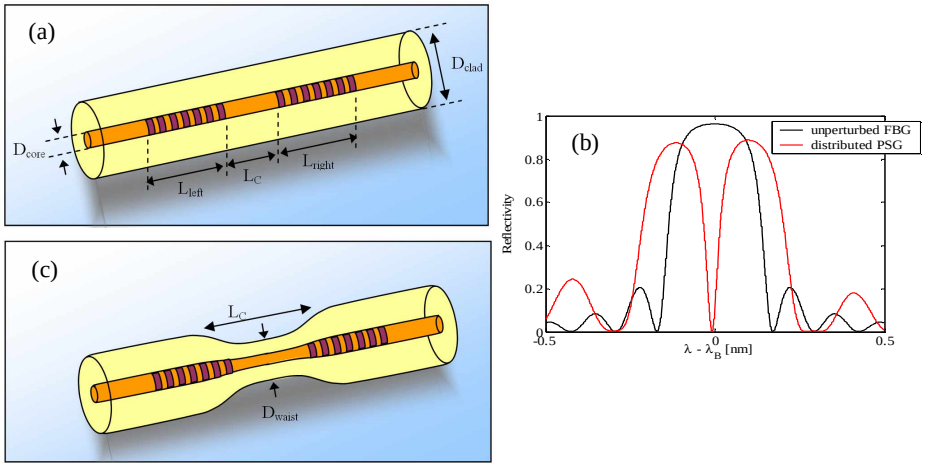

Fig. 1. (a), Schematic diagram (not in scale) of EAD-based interferometric structure; (b) Unperturbed FBG and distributed PSG spectra; and (c) Schematic diagram (not in scale) of grating with tapered cavity region.

Here, the simple erasure procedure obtained by the EAD technique is properly modified leading to the possibility to finely vary the propagating features (effective refractive index) and insertion losses in the defect cavity through the modification of the fiber shape within the erased region. To this aim, successive electric discharges opportunely combined with a fiber

#97128 - $15.00 USD Received 5 Jun 2008; revised 30 Jul 2008; accepted 30 Jul 2008; published 15 Sep 2008

pulling setup are adopted to not-adiabatically taper the fiber region in the erased region, leading to a fine fiber diameter decrease and a simultaneous cavity extension. A schematic diagram of the structure is shown in Fig. 1(c) which is characterized by a longitudinal extension of the cavity length L_C while the lowest diameter D_{waist} is referred to the middle of the tapered cavity.

The not-adiabatic nature of the taper combined with the correct selection of the spatial location of the taper along the grating region allows the full control of the cavity losses through the balancing of the mirrors reflectivity and thus enabling the control of the defect state within the grating PBG. In addition, the cavity extension and the effective refractive index changes due to core diameter reduction acts on the defect state positioning allowing the complete control of the band-gap modifications.

With regard the defect bandwidth, it is strongly related to the cavity finesse and thus can be tailored by a correct selection of the pristine grating features as demonstrated in the next sections.

3. Experimentals

Electric Arc-Discharge approach has been carried out by a commercial fusion splicer unit (Fujikura FSM-50S). A schematic diagram of the experimental set up is shown in Fig. 2(a). Two metallic loose-tubes allow the correct fiber arrangement between the splicer electrodes. Additionally, a micro-controlled translation stage is adopted to provide the correct positioning of the grating with respect to the electrodes enabling a fine control of the spatial location where the local grating erasure occurs. On the base of several experiments, fusion current and arc duration were manually selected to 17.1 mA and 100 ms, respectively, in order to achieve an electric arc that would locally heat and not-permanently distort the fiber.

Even if EAD technique represents a simple and low cost post-fabrication process [11], it exhibits some drawbacks limiting its use in practical applications. They can be resumed as follows:

i) Not repeatable arc discharge due to current inaccuracy and electrodes aging;
ii) Practical errors in the grating identification and in its positioning in respect to the electrodes location.

The immediate effect of these limitations leads to a poor control on the defect state spectral position and a weak degree of repeatability of the treatment at fixed process parameters. Moreover, small errors in the alignment of the grating center ($L_{left} \neq L_{right}$) are responsible for mirrors unbalance and thus for weak defect state within the grating PBG [11]. As matter of fact, these drawbacks make the simple EAD approach not suitable in practical application.

Here, we demonstrate the capability to control position and depth of the defect state by acting on the fiber shape and position of the erased region overcoming the aforementioned practical issues.

The tapering of the erased region has been achieved by adopting the setup before described while the fiber was kept under constant axial tension during the arc discharge. A small weight and a pulley have been used to reach specific values of the tension state (see Fig. 2(b)). In all experiments here illustrated, the process parameters (fusion current, arc duration and weight) were properly selected after an intense characterization on single-mode optical fibers.

The adopted fusion splicer was also equipped with a LCD monitor, which provides a real-time monitoring of the optical fiber in correspondence of the erased region. In addition, a video output terminal enables the acquisition of the digitalized images for the analysis of the obtained shape with a resolution of +/-1 μm.

A commercial 9 mm long standard uniform FBG UV written in SMF-28 fiber, demonstrating a peak reflectance of about 98%, a central wavelength of 1542.039 nm and a bandwidth Full Width Half Maximum (FWHM) of 0.198 nm was initially selected.

#97128 - $15.00 USD Received 5 Jun 2008; revised 30 Jul 2008; accepted 30 Jul 2008; published 15 Sep 2008

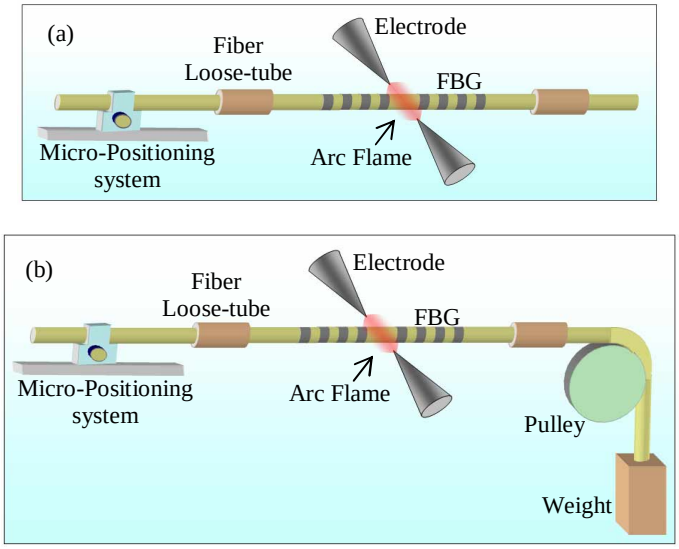

Fig. 2. Schematic diagram of the EAD setup: (a) localized grating erasure; (b) cavity tapering setup.

In order to analyse the capability to control the optical losses and their effect on the defect state depth an asymmetric positioning was chosen. To this aim, the EAD was located at 3 mm from the left end of the pristine grating, which in turn leads to a higher reflectivity for the lateral grating at the right of the tapered region (see Fig. 3(a)).

FBG reflected spectra were recorded by a simple optoelectronic setup with a wavelength resolution of 1 pm involving a tunable laser source (Ando AQ4321D) to radiate the grating and an optical spectrum analyzer (Ando AQ6317C) to collect the reflected spectrum from the grating. In addition, the overall transmitted power was monitored by using operating wavelengths out from the grating bandwidth. It is worth noting that FBG reflected spectra were recorded by radiating the grating structure from the left side with respect to the tapered region.

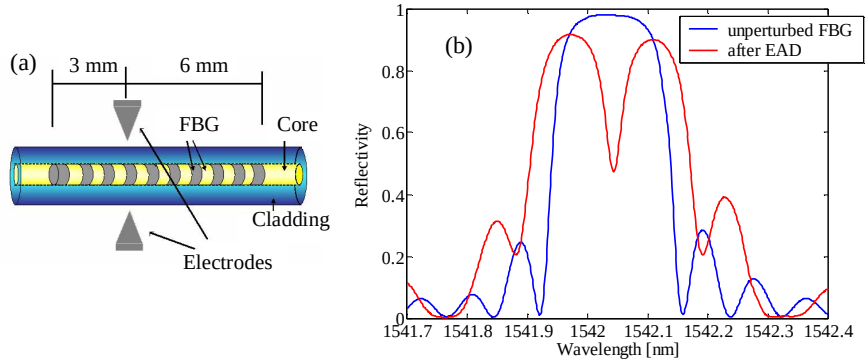

Fig. 3. (a) Schematic arrangement of grating between electrodes; and (b) Unperturbed and EAD-treated FBG spectra.

3.1 Effects of the local taper

In Fig. 3(b) the spectral response of the FBG treated by asymmetric EAD without weight is compared with the response of the pristine device. As expected, the reflected bandwidth increases from 0.198 to 0.270 nm due to the minor length of the lateral gratings compared with the length of the pristine device. Besides, the reflected spectrum demonstrates the

#97128 - $15.00 USD Received 5 Jun 2008; revised 30 Jul 2008; accepted 30 Jul 2008; published 15 Sep 2008

formation of the defect state at 1542.043 nm with a 3 dB bandwidth of 41 pm and a minimum reflectivity of about 47.5%. At the same time, the weak depth of the defect state can be clearly explained by considering the asymmetric positioning of the EAD leading to an unbalance between the lateral mirrors of the thermally induced cavity.

Besides, to demonstrate the capability to compensate this unbalance through the control of the optical losses introduced by tapering the erased region, successive EADs were carried out while a small mass was applied to the free fiber (Fig. 2(b)). For these successive EADs, arc duration of 200 ms and electric current of 14.0 mA were selected to properly control the taper waist. Figure 4 shows the waist diameter as function of the arc discharge number (N_{ARC}) obtained by using the aforementioned process parameters. Here, N_{ARC}=0 is referred to pristine grating while N_{ARC}=1 corresponds to the first EAD without applied weight. Step-by-step, the applied weight was adjusted from 12 gr. to 4 gr. in order to obtain a quasi linear diameter decreasing with a tapering rate of approximately 19 μm/arc.

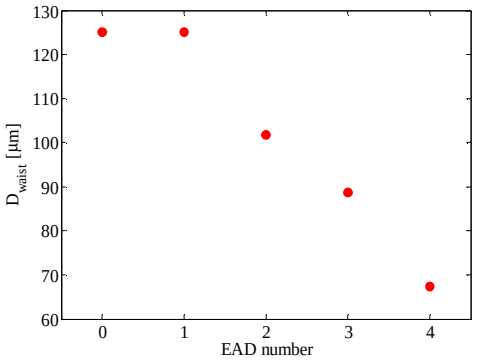

Fig. 4. D_{waist} as function of arc-discharge number during the tapering process.

Figure 5(a) shows the spectral response of the device in the case of waist diameter of 102 μm whereas an image of the tapered structure is shown in Fig. 5(b). As observable, a full defect state centred at 1541.995 nm and characterized by a 3 dB bandwidth of 77 pm was achieved leading to a reached balance between the lateral mirrors caused by the optical losses introduced by the not adiabatic nature of the local taper.

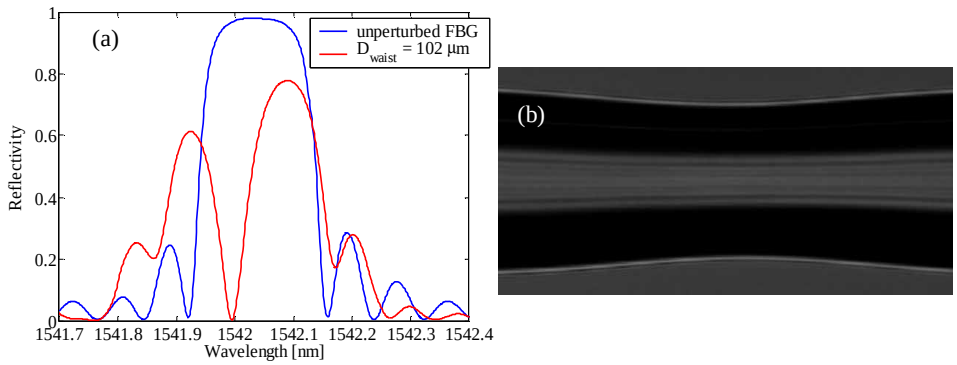

Fig. 5. (a). Spectral response in case of D_{waist}= 102μm and L_C= 460μm compared with pristine spectrum; and (b) Image of tapered fiber in case of D_{waist}= 102μm and L_C= 460μm;

It is worth to note that an additional effect of the optical losses is a decrease of the overall power reflected which is in good agreement with value of 1.8 dB registered by measuring transmitted power out from the device bandwidth for a waist diameter of 102 μm. Figure 6 resumes the behaviour of power losses and defect state reflectivity as function of the fiber diameter in the tapered region. As evident, in the case of waist diameter of 102 μm, the power

#97128 - $15.00 USD Received 5 Jun 2008; revised 30 Jul 2008; accepted 30 Jul 2008; published 15 Sep 2008

losses in the cavity enable the reaching of a full defect state, while further diameter decrease forces higher power losses and thus a reverse unbalancing leading to a diminution of the defect state depth.

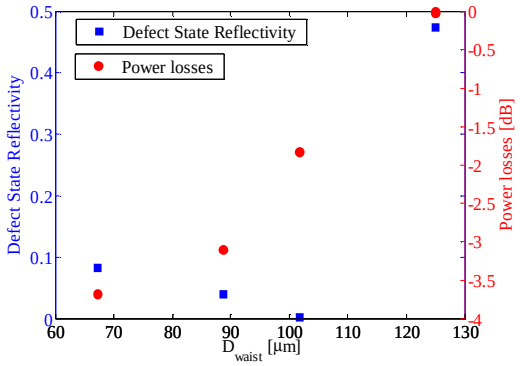

Fig. 6. Defect State Reflectivity and Power losses as function of waist diameter.

On the base of these results, the proposed method seems to work correctly enabling an efficient tailoring of the defect state depth and wavelength. It well combines the simplicity of EAD-based post-fabrication approach to force distribute phase-shift demonstrated in Ref. [11] with a tailoring mechanism never investigated on Bragg grating to the best of our knowledge. It is worth noting that here a worst case is investigated where a strong unbalancing was properly forced at the first stage. It is reasonable to assume that in practical cases, the unbalance due to a quasi correct positioning of the erased cavity in the middle of the grating structure can be compensated by a slight change of the fiber diameter avoiding significant losses in the overall grating response. Finally, when obtained the balance point, the spectral position of the defect state can be easily adjusted by slightly changing (few microns) the taper waist enabling the modulation of the distributed phase shift without affecting the power losses.

3.2 Effect of the grating features

In order to outline how the choice of the grating features influences the characteristics of the defect state, a similar experiment has been carried out by using a "strong" FBG. To this aim, a commercial 9 mm long FBG, UV-written in SMF-28 fiber, demonstrating a central wavelength of 1558.018 nm, maximum reflectivity of 100% and a bandwidth FWHM of 0.327 nm was selected. In this case, the grating was arranged in the splicing machine with the electrodes positioned as schematically shown in Fig. 7(a) with L_{left} and L_{right} approximately of 4 and 5 mm, respectively. The EAD procedure was characterized by an arc duration of 100 ms and an electric current of 17.1 mA.

Figure 7(b) shows the spectral response of the pristine FBG and after the first EAD without tapering the erased cavity. Accordingly with previous experiment, an increase in the reflected bandwidth of 75 pm and the formation of an ultra narrow defect state at 1557.932 nm exhibiting minimum reflectivity of 8.5% and bandwidth of 5 pm evaluated at 3 dB.

The reason for an ultra narrow defect state can be attributed to the higher reflectivity of the cavity mirrors able to induce high finesse interferometer. This means that ultra narrow spectral signatures can be achieved by an adequate choice of the grating features opening up the possibilities to realize with this simple post processing technique advanced in fiber filters for telecommunication applications. It is important to remark that the post processing technique is wavelength independent and can be applied to gratings with very different operating wavelengths.

Also in this case, the effects of the cavity tapering on the defects state features have been investigated. To this aim, successive EADs were performed along the same grating region and the fabrication parameters were adjusted to achieve a finer control of the waist diameter.

#97128 - $15.00 USD Received 5 Jun 2008; revised 30 Jul 2008; accepted 30 Jul 2008; published 15 Sep 2008

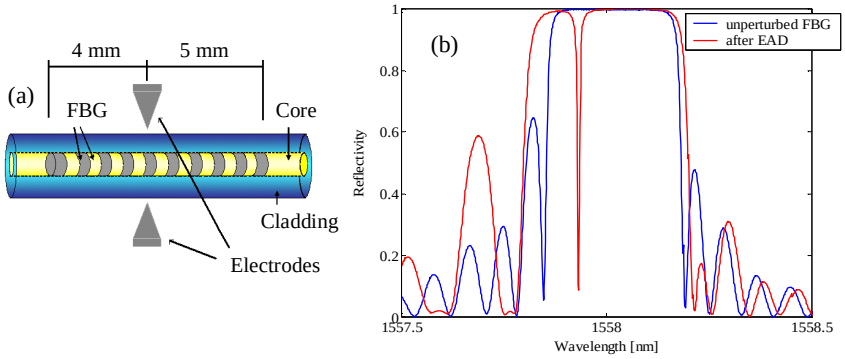

Fig. 7. (a) Schematic arrangement of grating between electrodes; and (b) Unperturbed, EAD-treated and tapered strong FBG spectra.

It is worth noting that the fine tapering process acts as an efficient tool enabling a full control of the FBG spectral features, in terms of capability to tune the defect state at specific wavelengths. For instance, Fig. 8(a) (red line) shows the reflected spectrum in case of D_{waist}=122μm (L_C=310 μm) where the defect state is centered with regards to the FBG bandwidth. Further thinning in the tapered region would induce additional cavity losses with consequent increase in the defect state depth. Figure 8(a) (blue line) plots the spectral response in case of D_{waist}=118 μm (L_C=345 μm) where a defect state reflectivity of 5.9% was achieved.

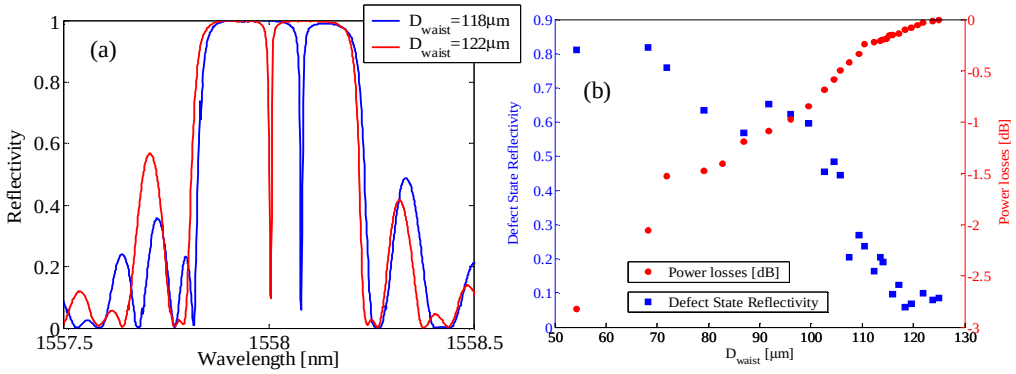

Fig. 8. (a). FBG reflected spectrum in case of D_{waist}=122μm and D_{waist}=118μm; and (b) Power losses and defect state reflectivity as function of waist diameter.

Figure 8(b) compares the power losses and the defect state reflectivity as function of the taper waist. Due to the weak unbalance before tapering, by further decreasing the fiber diameter, a diminution of the defect state depth occurs due to the reverse unbalance induced by the increase of the cavity losses.

As matter of fact, experimental evidence confirms the capability to completely control the spectral behavior of the post processed device, additionally, a proper selection of the pristine grating features plays a fundamental role in the determination of the defect state bandwidth with great potentialities for telecommunication applications.

3.3. Effect of strain and temperature

In this section, we report on the effects of strain and temperature on the spectral response of locally tapered FBGs.

#97128 - $15.00 USD Received 5 Jun 2008; revised 30 Jul 2008; accepted 30 Jul 2008; published 15 Sep 2008

3.3.1 Strain effect

In the former case, to correctly characterize the grating behaviour versus strain during the multi-step tapering process maintaining the process spatial self-referencing, a proper procedure was implemented. After each EAD, the strain characterization has been carried out by changing the weight used for stretching the fiber during the tapering process in the range 0-40 gr. (see Fig. 2(a)). Here, a 9 mm long FBG centered at 1542.005 nm with a bandwidth FWHM of 310 pm and maximum reflectivity of 100% was selected whereas the electrodes position was fixed at 3.0 mm from the left grating end.

Figure 9 plots the strain characterization in terms of the Bragg wavelength (λ_B) (centroid wavelength) versus the applied weight before the thermal treatment. As expected, it exhibits a linear behaviour revealing a sensitivity of 10.7 pm/gr. The graph also reports the behaviour of the wavelengths corresponding to the left and right edges of the grating spectrum evaluated at 50% of the FBG maximum reflectivity, λ_L and λ_R respectively. As expected, the spectrum moves unaltered towards longer wavelengths as the weight is increased.

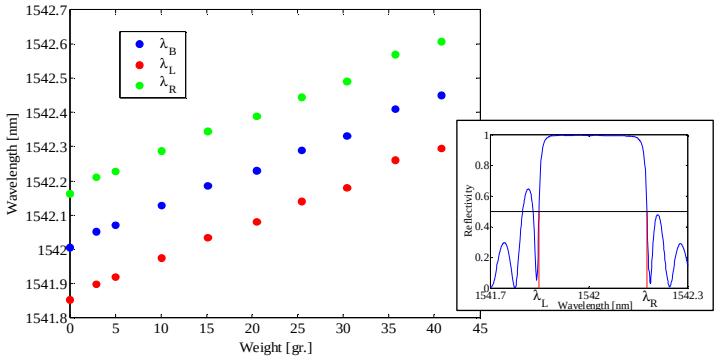

Fig. 9. Strain characterization of the bare FBG: λ_L and λ_R have been individuated as reported in the inset figure.

The same characterization has been repeated after the first EAD without tapering. In this case, due to the defect state formation, the strain sensitivity was retrieved taking in consideration the defect wavelength and the wavelengths at the spectrum edge according to the previous case. This characterization was repeated after each EAD involving also the local tapering of the erased region.

Figure 10(a) shows the defect state wavelength (λ_{DS}), λ_L and λ_R, respectively, versus the applied weight in case of D_{waist} of 48 μm. As evident, the defect state wavelength linearly shifts towards higher wavelengths as the applied weight increases, with an improved sensitivity of 14.2 pm/gr. On the other side, λ_L and λ_R exhibit sensitivities of 10.7 and 10.5 pm/gr. respectively, very close to the pristine grating case. This means that for this value of the taper waist, the defect state wavelength exhibits an improved sensitivity in respect to the overall grating stop-band, which in turn results very similar to the sensitivity measure for the pristine device.

To better understand the differential strain sensitivity of the defect state in respect to the overall grating stop-band, we report in Fig. 10(b) the defect state sensitivity gain with respect to the pristine Bragg wavelength as function of the taper waist. Based on the results reported, it is evident that as the taper waist is diminished down to 90 μm the defects state sensitivity starts to increase in respect to the case of the pristine device. Finally, as the waist diameter reaches D_{waist}=48 μm, a sensitivity gain of 1.33 is achieved. This result can be explained by considering the increase of the strain state in correspondence of the local taper due to the diameter reduction for a given applied stress. Moreover, additional sensitivity improvements are expected by considering longer tapered regions.

#97128 - $15.00 USD Received 5 Jun 2008; revised 30 Jul 2008; accepted 30 Jul 2008; published 15 Sep 2008

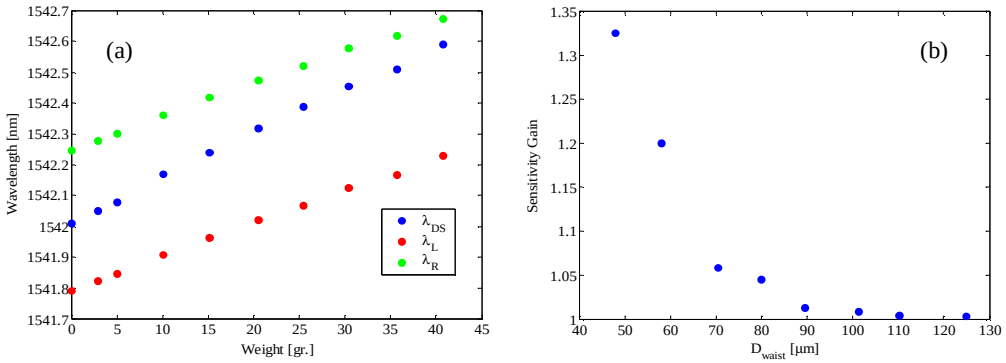

Fig. 10. (a). Strain characterization for D_{waist} = 48 μm; and (b). Sensitivity gain versus D_{waist}.

As matter of fact, the proposed structure should exhibit advantages for local strain measurements if compared with the pristine grating. First, the defect state exhibits a significant sensitivity gain for waist diameter ranging around 50 μm where a good fiber mechanical strength can be still envisaged for many structural applications. On the other side, the spectral shift of the defect state could be identified more easily than the unperturbed grating stop-band in light of its narrower spectral features, leading to advantages in terms of measurements resolution.

3.3.2 Temperature effect

With regards temperature effects, a simple experimental setup based on the use of Peltier cells capable to control the temperature with resolution of +/-0.1°C was adopted. A careful temperature characterization in the range 20-70°C was provided on the pristine grating and on the tapered grating structure with D_{waist} of 48 μm.

Figure 11(a) plots the centroid Bragg wavelength, λ_L and λ_R (as defined in insert of Fig. 9) related to the unperturbed grating as function of the local temperature. As expected, a linear spectral red shift is measured as the local temperature increases: λ_B, λ_L and λ_R exhibit the same thermal sensitivity of 9.7 pm/°C. Differently form the strain analysis, similar results have been also obtained in the case of minimum waist of 48 μm (see Fig. 11(b)) where a quasi rigid red shift of the grating spectral response was observed demonstrating sensitivities of 9.9, 9.8, and 9.6 pm/°C, for the defect state wavelength, λ_L and λ_R respectively.

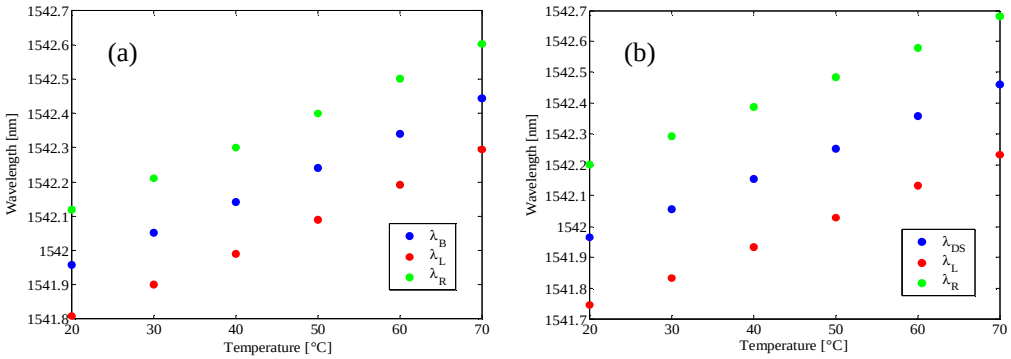

Fig. 11. Temperature characterization: (a) bare FBG; (b) D_{waist} = 48 μm.

As matter of fact, due to different spectral behaviour versus strain and temperature changes, the proposed structure could enable the possibility to realize temperature self-referenced strain measurements by a single sensing element eliminating the typical cross sensitivity of FBGs sensors. To this aim, both the defect state wavelength and one between λ_L

#97128 - $15.00 USD Received 5 Jun 2008; revised 30 Jul 2008; accepted 30 Jul 2008; published 15 Sep 2008

and λ_R have to be monitored. Considering D_{waist}=48 μm case, for example, Fig. 12 reports the difference λ_{DS} - λ_L in case of strain and temperature changes. As observable, as the applied weight passes from 0 to 40 gr. the wavelength difference passes from 220 pm to 362 pm, while it is constantly equal to 222+/-4 pm as the temperature varies in the range 20-70°C.

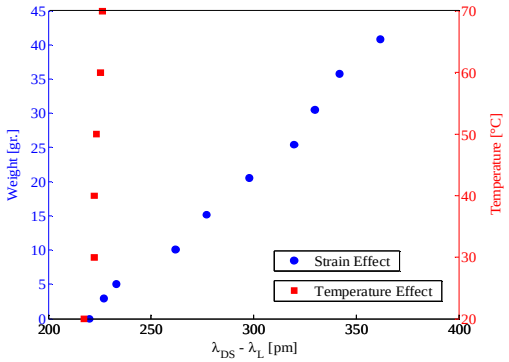

Fig. 12. Evolution of the difference between λ_{DS} and λ_L as function of strain and temperature.

The reported results confirm the effectiveness of such devices to be used for temperature self-referenced strain measurements. At the same time, suitable combination of strain and temperature actuation enables the possibility to realize tuneable narrow band filters for telecommunication applications where the defect state bandwidth can be easily tailored as demonstrated in previous sections.

4. Conclusion

In this work, a cost-effective post-processing approach to provide a full engineering of the photonic bandgap in UV written fiber grating devices has been experimentally demonstrated. Local thermal treatment combined with local tapering prove the great potentialities of the technique to provide new solutions for both sensing and telecommunication applications. The technique can be employed in case of fiber grating devices including long period gratings tilted and chirped FBGs where the refractive modulation is created by UV exposure. More complex structures are also envisaged by including more tapered regions along the grating length enabling the formation of new spectral features to be tailored for specific applications.

Acknowledgment

This work was supported by Italian “Ministero dell'Istruzione, dell'Università e della Ricerca (MIUR)”; project RBIP067375 (ASSO).

#97128 - $15.00 USD Received 5 Jun 2008; revised 30 Jul 2008; accepted 30 Jul 2008; published 15 Sep 2008